Wrexham University Research Online

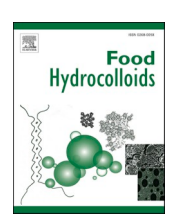
Journal Article
Hydrophobically modified sodium alginate for the encapsulation and controlled release of lutein
Han, L., Zhai, R, Williams P.A., Dong, N., Yang, J., and Hu,.B.
This article is published by Elsevier. The definitive version of this article is available at: https://www.sciencedirect.com/science/article/abs/pii/S0268005X25010690
Recommended citation:
Han, L., Zhai, R, Williams P.A., Dong, N., Yang, J., and Hu, B. (2025), 'Hydrophobically modified sodium alginate for the encapsulation and controlled release of lutein', Food Hydrocolloids, 172, 112109. doi: 10.1016/j.foodhyd.2025.112109

ELSEVIER

Contents lists available at ScienceDirect

Food Hydrocolloids

journal homepage: www.elsevier.com/locate/foodhyd



Hydrophobically-modified sodium alginate for the encapsulation and controlled release of lutein

Lingyu Han^{a,1}, Ruiyi Zhai^{a,1}, Peter A. Williams^{b,*}, Nuo Dong^a, Jixin Yang^b, Bing Hu^{a,**}

ARTICLE INFO

Keywords:
Sodium alginate
Hydrophobic modification
Long-chain fatty acyl chloride
Lutein
Targeted delivery

ABSTRACT

Amphiphilic derivatives of sodium alginate were generated by acylation with alkyl chains of varying lengths. These derivatives possessed the flexible sodium alginate chain and could self-assemble into globular-shaped micelles via hydrophobic interactions in aqueous solutions. Both the critical aggregation concentration and hydration diameters of the aggregates were reduced as the length of the hydrophobic chains increased at similar degrees of substitution, and increased alkyl chain lengths were associated with improved encapsulation efficiencies and loading capacities. Lutein-loaded micellar aggregates showed significantly increased environmental stability on exposure to temperature, UV, and visible-light radiation. The *in vitro* release of lutein from the aggregates followed the non-Fickian diffusion model. MTT assays indicated no marked cytotoxicity to RAW 264.7 cells at $1000~\mu$ g/mL concentration. Using lutein as a model, the potential of the micellar-like aggregates as hydrophobic carriers was assessed, demonstrating a correlation between lutein release and alkyl chain length. These findings demonstrate the potential of amphiphilic derivatives of sodium alginate with tunable structures and properties for applications in the food industry.

1. Introduction

Lutein, a natural carotenoid present in egg yolk and leafy green vegetables, serves as a crucial dietary component (Hao et al., 2022). However, it is easily degraded in the environment, leading to discoloration and reduced activity (Xu et al., 2023). The lutein structure contains 10 conjugated double bonds and is thus strongly hydrophobic, preventing its mixing with vesicles or micelles in the intestines and thus limiting its bioavailability and absorption (Zhang, et al., 2024). The bioavailability and absorption of lutein are enhanced when consumed with lipids, fats, and lipoproteins (Bhat et al., 2020). However, the escalating obesity epidemic, coupled with the high costs associated with energy-intensive emulsification equipment in the food industry, has spurred growing interest in the development of reduced-fat delivery systems (Li et al., 2020). New delivery systems capable of encapsulating lutein and protecting it from light, temperature, and other harmful environmental factors for use in food processing are thus needed.

The introduction of new hydrophobic molecules on active functional groups on polysaccharides has been found to produce amphiphilic

polysaccharide derivatives (Han et al., 2024). These derivatives tend to aggregate into micellar-like structures in aqueous solutions due to hyinteractions (Zhang, et al., polysaccharide-based micellar-like structures are useful biomaterials due to the combined properties of the biopolymer and the micelles (Atanase, 2021). These structures are typically biodegradable, non-toxic, and non-immunogenic and have high loading capacities, making them ideal as carriers of active substances (Wu et al., 2022). For example, a previous study (Han et al., 2022) reported that doxorubicin-loaded micelles of octenyl-succinylated inulins showed significant promise in the encapsulation, dissolution, and specific delivery of hydrophobic drugs, particularly anticancer agents. Liu, Ma, et al. (2024) prepared amphiphilic derivatives of oxidized sodium alginate with oleylamine via reductive amination formylation of Schiff bases, aiming to improve the bioavailability of β-carotene. A report by Zhang, et al. (2024) described the construction of burdock polysaccharides derivatized with stearic acid, forming lutein-loaded assembled aggregates to increase its transport through membranes. Sodium alginate, as a natural anionic polysaccharide, possesses excellent

^a College of Life Science, Dalian Minzu University, Dalian, Liaoning, 116600, China

^b Faculty of Life and Social Sciences, Wrexham University, Plas Coch, Mold Road, Wrexham, LL11 2AW, United Kingdom

^{*} Corresponding author.

^{**} Corresponding author.

E-mail addresses: Pete.Williams@wrexham.ac.uk (P.A. Williams), hubing19871121@163.com (B. Hu).

¹ The authors contributed equally to this work.

biocompatibility and biodegradability, but its high hydrophilicity limits its application in delivering lipophilic nutrients. Nevertheless, there has been minimal investigation into the potential of amphiphilic derivatives of sodium alginate modified with hydrophobic alkyl chains for the delivery of functional materials. By introducing alkyl chains of varying lengths, we aim to develop a tunable amphiphilic system capable of forming stable micelle-like aggregates and enabling controlled release of lutein. The structure-activity relationship between the chain length and functional performance would be explored, particularly in alginate-based delivery systems. This approach not only improves the environmental stability of lutein but also removes the necessity for high-fat additives, thereby supporting the growing demand for low-fat functional food products.

The present study describes the preparation of self-assembled micelle-like aggregates by synthesizing amphiphilic derivatives of sodium alginate through acylation with alkyl chains of varying lengths. The structure of hydrophobically modified sodium alginate with different alkyl chain lengths was characterized using Fourier-transform infrared spectroscopy (FTIR), ¹H nuclear magnetic resonance (¹H NMR), X-ray diffraction (XRD), and thermogravimetric analysis (TGA). Additionally, the solution and interfacial behavior of these derivatives were investigated, along with their efficacy in delivering and sustaining the release of lutein in the small intestine. The results indicate enhanced environmental stability and intestinal absorption of lutein. This study demonstrates that the modification of sodium alginate with alkyl chains of varying lengths represents a promising strategy for the development of lutein delivery systems, providing a potential reference for its application in food production.

2. Materials and methods

2.1. Materials

Sodium alginate (9 kDa molecular weight) was isolated and characterized as previously reported (Han et al., 2024). Octanoyl chloride (C8), decanoyl chloride (C10), dodecanoyl chloride (C12), myristoyl chloride (C14), formic acid, 3-(4, 5-dimethylthiazol-2-yl)-2, 5-diphenyltetrazolium bromide (MTT), lutein, and Tween 80 were purchased from the Macklin Biochemical Co., Ltd. (Shanghai, China). Additional reagents included pyrene (Shanghai Aladdin Biochemical Technology Co., Ltd., Shanghai, China), deuterium oxide (D2O, Alfa Aesar Co., Ltd. (Shanghai, China), phosphate-buffered saline (PBS) at pH 7.4 was procured from Sangon Biotech Co., Ltd. based in Shanghai, China. Dimethyl sulfoxide (DMSO), hydrochloric acid (HCl), sodium hydroxide (NaOH), absolute ethanol, and potassium bromide (KBr) were obtained from Tianjin Kemiou Chemical Reagent Co., Ltd., situated in Tianjin, China. The RAW 264.7 cell line was obtained from the Cell Bank of the Chinese Academy of Sciences (Shanghai, China). Meanwhile, the cell culture reagents, including DMEM, penicillin-streptomycin solution, and fetal bovine serum (FBS), were purchased from Gibco, a subsidiary of Thermo Fisher Scientific in the United States.

2.2. Synthesis of sodium alginate derivatives with various alkyl chain lengths

In the acylation process, a 1 % (w/v) sodium alginate solution (100 mL) was first blended with 10 mL of formic acid and incubated at 25 °C temperature for 30 min. Subsequently, 15 mL of octanoyl chloride, 13 mL of decanoyl chloride, 10 mL of dodecanoyl chloride, or 8 mL of myristoyl chloride was added dropwise to the mixture, which was then stirred at 50 °C for 30 min. To terminate the reaction, ethanol was incorporated, and the resulting mixtures were subjected to filtration to obtain various sodium alginate derivatives. The harvested precipitates were subjected to dialysis (molecular weight cutoff: 3500 Da) against deionized water over a three-day period to eliminate trace residual reagents and secondary products. The material was then freeze-dried,

resulting in sodium alginate derivatives with different alkyl chain lengths, termed ALG-C8, ALG-C10, ALG-C12, and ALG-C14.

2.3. Characterization of the derivatives

2.3.1. ¹H nuclear magnetic resonance (NMR) spectroscopy

Spectra were acquired on an ULTRASHIELD 400 PLUS system (Bruker, USA) at 25 $^{\circ}$ C, a frequency of 400 MHz, and with deuterated water (D₂O) as the solvent.

2.3.2. Fourier-transform infrared (FTIR) spectroscopy

The spectra of sodium alginate and its derivatives were acquired with a FTIR spectrometer (Shimadzu, Japan) using a KBr pellet over the 500-4000 $\rm cm^{-1}$ range. 64 spectral scans at 4 $\rm cm^{-1}$ resolution were collected.

2.3.3. Thermogravimetric analysis (TGA)

Thermal characteristics were assessed by a TGA (SDT 650, TA, USA) system, where the samples were heated at the range of 30–600 $^{\circ}\text{C}$ at 20 $^{\circ}\text{C/min}.$

2.4. Critical aggregation concentration (CAC)

2.4.1. Fluorescence

The critical aggregation concentrations (CACs) were measured using a pyrene fluorescent probe following an established protocol (Han et al., 2024). A solution of pyrene in methanol was mixed with varying concentrations of the derivatives to a final concentration of $1\times 10^{-6}\ mol/L$ of pyrene and left to stand at 25 °C overnight. Fluorescence emission spectra were recorded using an FS5 spectrofluorometer produced by Edinburgh Instruments (UK).

2.4.2. Surface tension (ST)

The static surface tension (ST) was measured in triplicate using a surface tension hmeter (model BZY-1, HengPing, Shanghai, China) at a temperature of $25\pm1\,^{\circ}\text{C}$. The CAC value was derived from the slope of a graph illustrating yield concentrations against equilibrium surface tension. The Gibbs adsorption equation (below) was used to calculate the molecular area (A) and the surface excess (Γ):

$$\Gamma = -\frac{1}{RT} \frac{d\gamma}{d \ln c} \tag{1}$$

$$A = \frac{1}{\Gamma N} \tag{2}$$

where, R represents the gas constant, N denotes Avogadro's number, γ corresponds to surface tension (ST), T signifies temperature, and C indicates concentration.

2.5. Zeta potentials and sizes of micellar-like aggregates

The above parameters were determined using a Zetasizer Nano ZS instrument (Malvern Instruments, UK) at a constant temperature of 25 °C. Samples were prepared at a concentration of 2 mg/mL, filtered through a 0.45 μm membrane filter, and measured in triplicate to determine the particle size. Additionally, the zeta potential values of the 2 mg/mL sample solutions in deionized (DI) water (pH 6.35) were determined under the same temperature condition of 25 °C.

2.6. Preparation and analysis of lutein-loaded aggregates

Solutions of sodium alginate derivatives ($100.0\,\text{mg}$) in $50\,\text{mL}$ DI were prepared after which $5\,\text{mL}$ lutein in ethanol ($3\,\text{mg/mL}$) was treated with probe-type ultra sonicator (SCIENTZ-IID, Scientz, Ningbo, China) for $30\,\text{min}$ at $30\,\text{W}$, before dialysis (MW cutoff $3500\,\text{Da}$) for $48\,\text{h}$ against DI to eliminate free lutein and residual solvent. The samples were then freezedried and subsequently dissolved in ethanol ($1\,\text{mg/}10\,\text{mL}$) with

sonication for 30 min. The absorbances at 445 nm were measured with a UV–vis spectrophotometer (UV-6100, MAPADA, China) and the lutein concentrations in the aggregates were determined using a standard calibration curve. The calibration curve was drawn by measuring the absorbance of ethanolic lutein solutions (free lutein) of known concentration (Fig. S1 in supplementary data). The encapsulation efficiency (EE) and loading capacity (LC) were computed using Equations (3) and (4), respectively:

$$EE (\%) = \frac{\text{weight of lutein in micellar} - \text{like aggregates}}{\text{weight of lutein fed initially}} \times 100\%$$
 (3)

$$LC~(\%) = \frac{\textit{weight of lutein in micellar-like aggregates}}{\textit{weight of micellar-like aggregates containing lutein}} \times 100\%$$

(4)

2.7. Micromorphological analysis

The morphological features of the aggregates were assessed via transmission electron microscopy (TEM) using a JEM-2100 instrument (JEOL, Japan). One drop of sample solution was A drop of the sample solution was put on a carbon-coated copper mesh before air-drying and negative staining with phosphotungstic acid (60 s). Aggregate sizes were determined using ImageJ.

2.8. Stability of lutein and lutein-loaded micellar-like aggregates

The effect of environmental factors on lutein stability in the aggregates was assessed as previously described (Fan, Gan, Zhang, & Yi, 2024, Fan et al., 2024; Li et al., 2024; Liu, Ma, et al., 2024).

2.8.1. Stability on storage

The impact of storage length on free and aggregate-loaded lutein was assessed by storing the samples in clear centrifuge tubes for 4 weeks at 25 $^{\circ}$ C. After extraction in ethanol, the lutein concentration was evaluated using a UV–vis spectrophotometer and the retention ratio was determined according to Equation (5)

Retention ratio of lutein (%) =
$$\frac{R1}{R2} \times 100\%$$
 (5)

where R1 and R2 represent the retained and initial lutein amounts, respectively. The degradation rate constant (k) and half-life $(t_1/2)$ were derived from the first-order kinetic equation, as specified below:

$$\ln\left(\frac{C}{C_0}\right) = -kt \tag{6}$$

$$t_{1/2} = \frac{\ln 2}{k} \tag{7}$$

where C_0 and C represent the amounts of lutein on days 0 and t, respectively.

2.8.2. Thermal stability

Free lutein and lutein-loaded micellar-like aggregates were incubated in water baths at 25, 37, 50, 65, 80, and 100 $^{\circ}$ C for 30 min. Absorbances were measured in a UV spectrophotometer to assess lutein retention and thus thermal stability.

2.8.3. Stability in UV light

Samples of free lutein and lutein-loaded aggregates were placed under UV light (30 W) for 0, 20, 40, 60, 90, 120, and 180 min at 25 $^{\circ}$ C. The percentage of lutein retention was assessed as described in Section 2.8.1.

2.9. In vitro lutein release

Lutein release *in vitro* was assessed by dialysis, as described by Liu, Ma, et al. (2024). While using this method, the pores of the dialysis membrane should be sufficiently large to allow the transfer of lutein but not the nanocarrier (Gupta et al., 2021). Specifically, 1.0 mL micellar-like aggregate solutions loaded with 0.1 mg lutein were dialyzed (MWCO 7000 Da) against PBS (30 mL, pH 7.4) with 0.5 % (w/v, g/mL) Tween 80 within a 37 °C water bath under rotation at 100 rpm. At specific times, 1.0 mL aliquots of the release medium were collected and the remaining system was topped up with fresh medium to maintain a constant volume. Photodecomposition of lutein was prevented by covering the containers with aluminum foil. The degradation rate constant (k) and half-life ($t_1/2$) were derived from the first-order kinetic equation, as specified below:

$$E_{r} = \frac{V_{e} \sum_{1}^{n-1} C_{i} + V_{b} C_{n}}{m_{loaded\ lutein}} \times 100\% \tag{8}$$

where V_e is the sample volume (1.0 mL) collected from the release medium; V_b is the total volume (30 mL) of the release medium; C_i and C_n represent the lutein concentrations in the release medium at times i and n, respectively; n is the number of time points used for sample collection; mloaded lutein is the amount of lutein originally loaded in the aggregates. The kinetic parameters of lutein release were determined as:

Zero order:
$$Qt = kt$$
 (9)

First order:
$$Qt = 1$$
- $exp(-kt)$ (10)

Higuchi:
$$Qt = kt^{1/2}$$
 (11)

Ritger-Peppas:
$$Qt = kt^n$$
 (12)

where Qt is the amount of lutein released at time t; k is the rate of release; n is the release exponent (Yang et al., 2021).

2.10. In vitro cytotoxicity assay

The impacts exerted by sodium alginate and its derivatives on RAW 264.7 cells were evaluated via MTT assays. In particular, RAW 264.7 cells were maintained in DMEM medium supplemented with 10 % fetal bovine serum (FBS) and 1 % penicillin-streptomycin cocktail. The cells were plated into 96-well plates at a density of 1×10^4 cells per well. Following 24 h of incubation under standard culture conditions, the original medium was aspirated and replaced with fresh medium containing test samples at various concentrations (0, 200, 400, 600, 800, and 1000 $\mu g/mL$). After growth for 24 h, the PBS with 20 μL of MTT reagent (5 mg/mL) introduced for 4 h, followed by the removal of the solution and the addition of 150 μL of DMSO to each well. Absorbance values were measured at 490 nm utilizing a Synergy H1 microplate reader (BioTek, USA), and cellular viability was subsequently calculated by means of Equation (13):

100% Cell viability =
$$\frac{At - Ac}{Au - Ac}$$
 (13)

where, At and Au denote the absorbance values at 490 nm in the presence and absence of the sample, respectively, while Ac corresponds to the absorbance of the cell-free control.

2.11. Statistical analysis

Data are presented as the mean \pm standard deviation and were subjected to one-way analysis of variance (ANOVA) using SPSS software. A p-value less than 0.05 was regarded as statistically significant.

3. Results and discussion

3.1. Synthesis and analysis of sodium alginate derivatives

The derivatives were successfully synthesized with identical degrees of substitution (DS) through the introduction of alkyl chains of different lengths onto the sodium alginate backbone. The synthesis details are presented in Fig. 1a.

Proton nuclear magnetic resonance proton magnetic resonance (1H NMR) signals for sodium alginate and their respective derivatives are depicted in Fig. 1b. The sodium alginate spectrum shows peaks in the region of 3.2–4.0 ppm, indicative of chemical shifts in the hydrogens of the β -D-mannuronic and α -L-guluronic acid moieties. All the derivatives showed similar spectra. The resonance signals detected at chemical shifts of 0.8, 1.2, 1.6, and 2.4 ppm arose from protons within methyl (-CH₃) and methylene (-CH₂.) moieties, thereby verifying the successful conjugation of long-chain fatty acyl chlorides to sodium alginate. An additional resonance peak at 4.79 ppm corresponded to solvent water (D₂O). The degree of substitution (DS) values from a prior publication from our group (Han et al., 2024) are compared with the current findings listed in Table 1. The DS values, representing the alkyl chain: sugar unit molar ratios, were markedly similar among all the derivatives.

The FTIR spectra are shown in Fig. 1c. In the sodium alginate spectrum, a distinct absorption band at 3400 cm⁻¹ is ascribed to the stretching vibrations of hydroxyl (-OH) groups, while the peaks at 1645 and 1406 cm⁻¹ are associated with asymmetric and symmetric vibrational stretching of carboxylate (-COO-) groups, respectively (Liu, Ma, et al., 2024). The peak at 2920 cm⁻¹ was attributed to the stretching vibration of -CH₂- in the sodium alginate. Following the grafting of alkyl chains onto the sodium alginate backbone, the absorption peak at 2925 cm⁻¹ showed a stronger absorption and a new absorption band 2835 cm⁻¹, corresponding to the asymmetric and symmetric -CH₂- stretching vibrations due to the introduction of hydrophobic alkyl chains (Li et al.,

2023). The intensity of these peaks increased progressively with the length of the alkyl chain, indicating a greater abundance of methylene groups in derivatives with longer alkyl chains. The derivative spectra exhibited additional absorption bands at wavenumbers of 1739 and 1560 cm⁻¹, which can be ascribed to the generation of ester bonds (Han et al., 2024). These observed changes in the FTIR spectra verify the success of the inclusion of alkyl moieties on the alginate sodium matrix backbone.

The findings pertaining to thermal stability are depicted in Fig. 1d. Both sodium alginate and its derivatives showed initial weight loss between 60 and 120 °C, resulting from the volatilization of water, either encapsulated or adsorbed, within the samples. With the temperature rising from 200 to 300 °C, distinct decomposition characteristics became evident in both sodium alginate and its derivatives. This was caused primarily by the carbonation of carboxyls on the molecule and structural breakdown of polymers (Han et al., 2024). Compared to sodium alginate, the peaks associated with weight loss in the derivatives were observed to shift toward lower temperatures, indicative of reduced thermal stability. It was found that derivatives with longer alkyl chains underwent the greatest weight loss. These results indicate that the addition of alkyl chains led to a decrease in the crystal structure and hydrogen bonding capacity of the derivatives, thereby reducing their thermal stability. This outcome is consistent with our previous findings (Han et al., 2024, 2025). The results also indirectly suggest the success of alkyl chain grafting onto the sodium alginate.

3.2. Aggregate self-assembly

The CAC values of the derivatives were assessed by pyrene fluorescence, with the relationships between the fluorescence intensity I_1/I_3 ratio and the derivative concentration presented in Fig. 2a. At lower concentrations, the I_1/I_3 ratio approximated 1.8, representative of pyrene within polar aqueous media solutions. With increasing

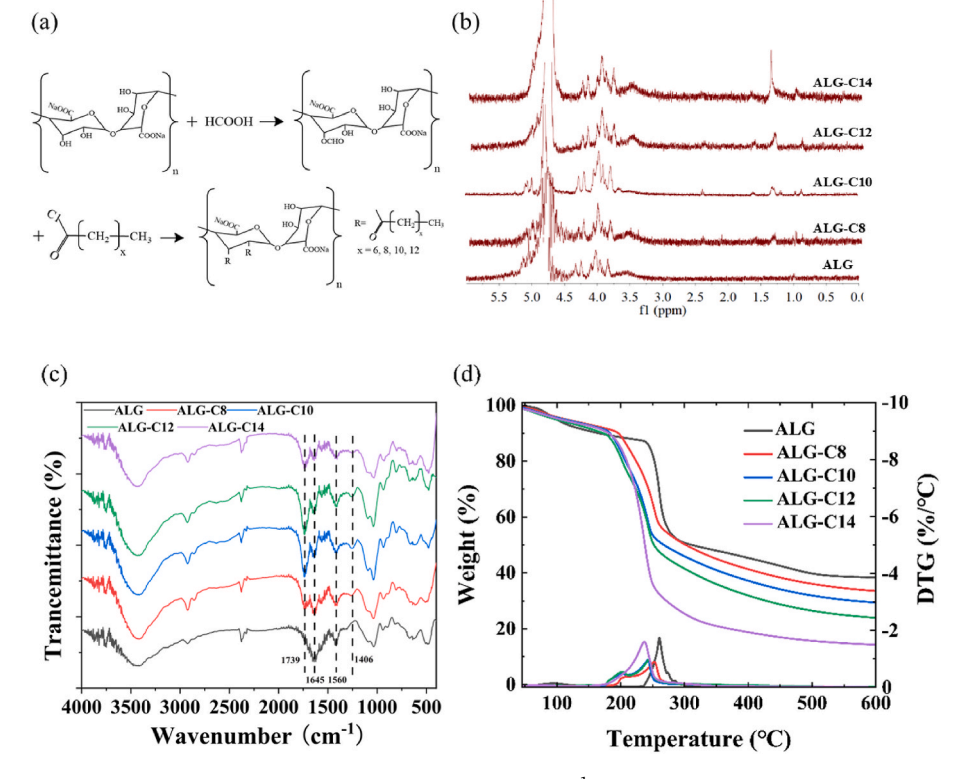


Fig. 1. (a) Synthesis of sodium alginate derivatives; (b) Proton nuclear magnetic resonance (¹H NMR) spectra of sodium alginate as well as its derivatives; (c) FTIR spectra of sodium alginate and its derivatives; (d) Thermogravimetric analysis (TGA) and derivative thermogravimetry (DTG) profiles of sodium alginate as well as its derivatives.

Table 1 Properties of aggregates.

Sample	DS (%)	CAC (mg/mL) Fluorescence measurement	CAC (mg/mL) ST	$\begin{array}{c} \Gamma \times 10^{-6} \\ \text{(mol/m}^2\text{)} \end{array}$	A (nm²)	Hydrodynamic diameter (nm)	Zeta potential (mV)	EE (%)	LC (%)
ALG-C8	$1.52\pm0.02^{\text{a}}$	1.40	$1.33\pm0.06^{\text{a}}$	0.09	0.18	195.8 ± 1.6^{a}	-33.7 ± 2.0^a	$43.90 \pm 0.54^{\rm d}$	$4.89\pm0.07^{\rm d}$
ALG-	1.52 ± 0.04^a	0.80	0.82 ± 0.03^{b}	0.10	0.17	184.8 ± 1.4^{b}	-33.3 ± 1.4^a	56.75 ± 2.16^c	7.84 ± 0.28^c
C10									
ALG-	1.56 ± 0.01^a	0.40	0.33 ± 0.06^{c}	0.12	0.14	155.0 ± 1.7^{c}	-33.7 ± 0.8^a	$73.41 \pm 1.48^{\mathrm{b}}$	$9.92\pm0.18^{\mathrm{b}}$
C12									
ALG-	1.56 ± 0.01^a	0.10	$0.09\pm0.01^{\rm d}$	0.14	0.12	$134.8\pm1.7^{\rm d}$	-32.1 ± 1.1^{a}	89.02 ± 1.58^a	11.78 ± 0.18^a
C14									

Annotation: Data are presented as mean \pm SD (n = 3). Different lowercase letters represents the significant difference (p < 0.05).

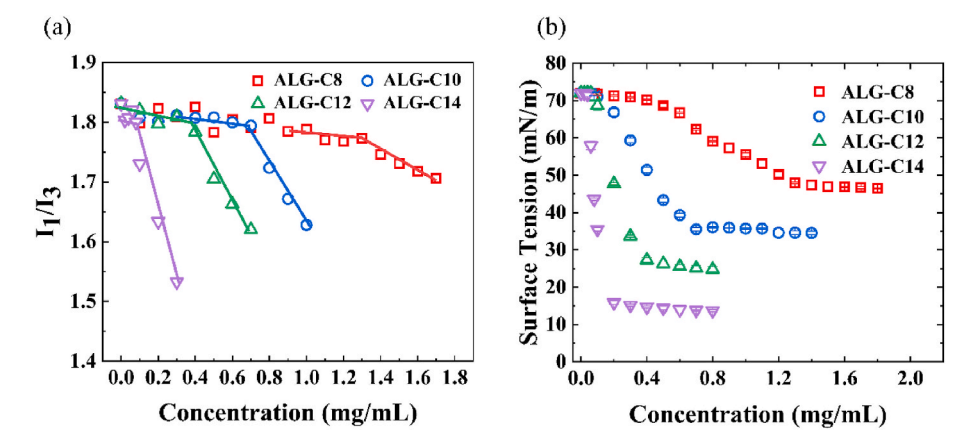


Fig. 2. (a) Intensities of pyrene fluorescence (I_1/I_3) in derivatives of varying concentrations; (b) Surface tension of derivatives of varying concentrations. Data are shown as mean \pm SD (n=3).

concentrations of the derivatives, the I_1/I_3 ratio decreased, signifying the formation of micellar-like aggregates featuring hydrophobic internal cavities that encapsulate pyrene, consistent with findings reported for amphiphilic block copolymers (Han et al., 2024). All curves exhibited analogous characteristics which was that the I_1/I_3 ratio stayed nearly unchanged at low sample concentrations, whereas it declined markedly with increasing concentrations. The inflection points of the curves were consistent with the critical aggregation concentration (CAC) values of the derivatives. Plotting the I_1/I_3 values versus the concentrations of the derivatives yielded CAC values of 1.4, 0.8, 0.4, and 0.1 mg/mL for ALG-C8, ALG-C10, ALG-C12, and ALG-C14, respectively. It is usually considered that the CAC values decrease as the lengths of the alkyl chains increase, as was noted in our earlier study on OSA-inulin (Han et al., 2017).

The ST is key for determining the surface activities of amphiphilic molecules, while CAC is an important indicator of changes from a dispersed to an aggregated state. In the dispersed state, the derivatives were dispersed homogenously in the water, thus increasing their surface areas within the solution. Thus, the ST value decreases as the derivative concentration increases. In the aggregated state, it is not possible to reduce the ST further by increasing the derivative concentrations. The CAC values of the derivatives are indicated by the inflection point on the ST profiles (Table 1 & Fig. 2b). The surface excess (Γ) denotes the concentration disparity between the interfacial region and bulk phase solution arising resulting from adsorptive behavior, sectional area (A) refers to the area occupied by a single molecule at the interface (Liu et al., 2020). The surface excess Γ value is obtained from the slope of they-ln C curve immediately below the CAC, as illustrated in Fig. S2 of the supplementary data. Derivatives bearing alkyl chains of different lengths displayed surface excess values in the range of 0.09–0.14 \times 10⁻⁶ mol/m², with the molecular cross-sectional areas varying from 0.12 to 0.18 nm² (as shown in Table 1). Among these derivatives, ALG-C14, which possesses the longest alkyl chain, exhibited the maximum Γ

value accompanied by the minimum A value. Such a combination of a large Γ value and a small A value indicates that surfactant molecules are densely packed at the air-water interface (Han et al., 2024). It is thus proposed that alkyl chain length influenced both the adsorptive capacity and packing density of the derivatives at the interfacial region, characterized by the surface-related parameters (CAC, surface tension, Γ , and A).

3.3. Characterization of sodium alginate derivatives and luteinencapsulated sodium alginate derivative aggregates

Table 1 presents the hydrodynamic diameters along with zeta potential potentials exhibited by micellar-type aggregates at a concentration of 2.0 mg/mL. With identical degrees of substitution (DS), an increase in alkyl chain length was accompanied by a decrease in aggregate size, ranging from 195.8 ± 1.6 to 134.8 ± 1.7 nm. These discrepancies could be attributed to differences in hydrophobic interactions between polymers featuring alkyl side chains of varying hydrophobic lengths, with longer chains associated with stronger interactions and thus reduced hydrodynamic diameters (Shen et al., 2021).

Zeta potentials play a significant role in the stability of micelles; generally, values exceeding 30.0 mV are a sign of enhanced stability, which arises from electrostatic repulsion. (Han et al., 2024). The surfaces of aggregates are featured by a strong negative charge, which is attributed to the carboxyl groups in the sodium alginate structure. (Liu et al., 2021). As can be seen from Table 1, the zeta potential values for all specimens are higher than 30.0 mV, which implies that the aggregates possess superior colloidal stability.

The LC and EE values of the samples are also shown in Table 1. It is evident that with increasing alkyl chain length, both the loading capacity (LC) and encapsulation efficiency (EE) of the aggregates exhibited a corresponding increase. The maximum LC and EE values were

observed in the lutein-loaded ALG-C14 aggregates, which were estimated to be 11.78 \pm 0.18 % and 89.0 \pm 1.58 %, respectively. In contrast to our previous observations (Han et al., 2025), the ALG-C8 sample—featuring a comparable degree of substitution (DS) of 1.54 \pm 0.04 % and an identical molar mass of 9 kDa—exhibited EE and LC values of 46.11 \pm 2.22 % and 4.61 \pm 0.22 %, respectively. For ALG-C8, the respective values of EE and LC were 43.90 \pm 0.54 % and 4.89 \pm 0.07 %, which were in agreement with our earlier observations. The observed decrease in critical aggregation concentration (CAC) with increasing chain length (Table 1) suggests an enhanced tendency for self-assembly and greater thermodynamic stability of the resulting aggregates (Han et al., 2024). This phenomenon facilitates the formation of a more stable hydrophobic core, thereby enabling more efficient incorporation and retention of lutein molecules. Additionally, the increase in surface excess (Γ) and the corresponding reduction in molecular cross-sectional area (A) for longer-chain derivatives (e.g., ALG-C14) indicate a more compact arrangement of surfactant molecules at the interface. This densely packed molecular structure promotes the formation of aggregates with smaller hydrodynamic diameters (as presented in Table 1), which exhibit larger specific surface areas and, consequently, enhanced embedding capacities (Han et al., 2024). These findings suggest that an extended hydrophobic chain resulted in intensified hydrophobic interactions, which promoted more robust binding of lutein molecules within the micellar core and consequently elevated both the LC and EE (Shen et al., 2021). Consequently, the superior performance of ALG-C14 in EE and LC can be directly attributed to its low CAC, high Γ , and small A values, all of which contribute synergistically to the formation of stable and compact aggregates with strong lutein affinity.

Transmission electron microscopy (TEM) micrographs illustrating the morphological features of both blank aggregates and lutein-encapsulated aggregates (at a concentration of 2.0 mg/mL) are shown in Fig. 3. The images demonstrate superior dispersibility, with no signs of aggregation observed. The average sizes of the aggregates were found to be 24.7, 21.4, 17.9, and 14.7 nm, respectively, in the case of derivatives with progressively longer alkyl chains, which is in line with the outcomes obtained from dynamic light scattering (DLS) analyses (Table 1). The aggregate sizes were found to be influenced by the lengths of the alkyl chains, whereas the particle sizes of the aggregates showed a

negative correlation with the chain lengths. However, it was observed that the particle sizes determined by TEM were less than those found using DLS; the reason is that the particles evaluated by TEM were completely dry, and dry aggregates are likely to undergo shrinkage due to water evaporation. In contrast, aggregates in solution were larger due to the presence of water molecules surrounding them, increasing their particle sizes relative to those seen in the dry state (Liu, Ma, et al., 2024). For lutein-loaded aggregates, their average sizes were 40.3, 33.1, 25.6, and 22.8 nm respectively with the increase in chain lengths, and these values were marginally larger than those of the blank aggregates, which has also been observed in our previous studies (Han et al., 2022, 2024, & 2026). This phenomenon may be attributed to the incorporation of lutein into the inner core of the micellar-like aggregates. The incorporation of lutein leads to an expansion of the hydrophobic core volume, resulting in a swelling effect and consequently an increase in the overall particle size. These results suggest that the lutein was successfully encapsulated within the micellar-like aggregates. Moreover, as found by Liu, Ma, et al. (2024), aggregates with sizes within a reasonable range of 20-200 nm demonstrated favorable penetration capabilities and could release functional active ingredients continuously, thereby exerting prolonged effects. Therefore, the micellar-like aggregates of ALG derivatives have significant potential for application in the fields of functional foods and biomedical engineering.

3.4. Comparative study of physicochemical stability

The effect of the aggregates on lutein stability was assessed by examining lutein retention under different environmental conditions, specifically, light, temperature, and length of exposure to UV irradiation. The relationship between lutein retention and storage time was determined to evaluate the photostability of different micellar-like aggregates. Fig. 4a illustrates the stability of free and encapsulated lutein when exposed to light. The sample colors and absorbances are presented in Fig. 4e. It can be seen that after seven days, only 44.5 % of the free lutein was present, while the lutein proportions in the aggregates were 60.0 %, 72.6 %, 79.8 %, and 87.6 %, respectively. Extended light exposure led to marked reductions in the retention of free lutein, with complete decomposition apparent by day 28. In contrast, the rates of

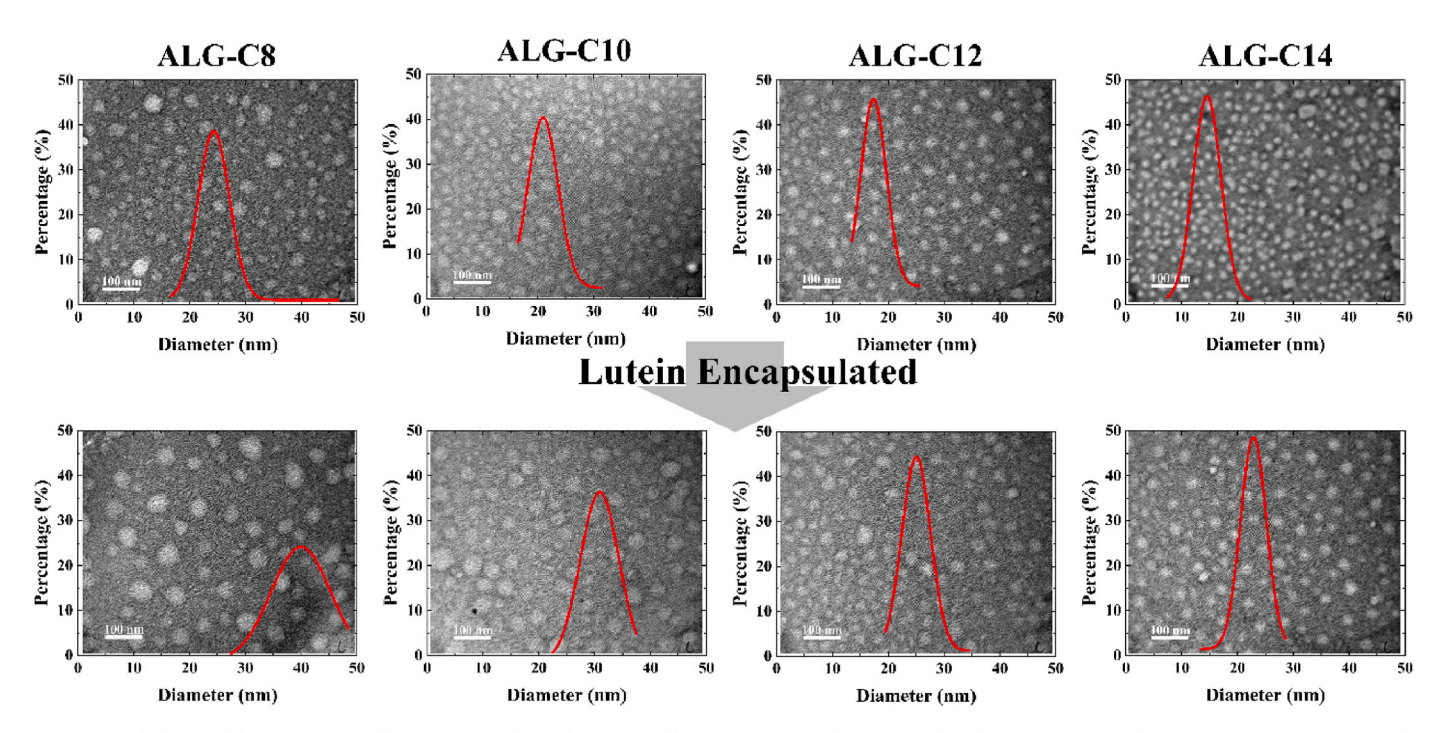


Fig. 3. Morphology of blank (upper) and lutein-encapsulated (lower) micelle-mimetic assemblies, as visualized via transmission electron microscopy (TEM). Scale bar: 100 nm.

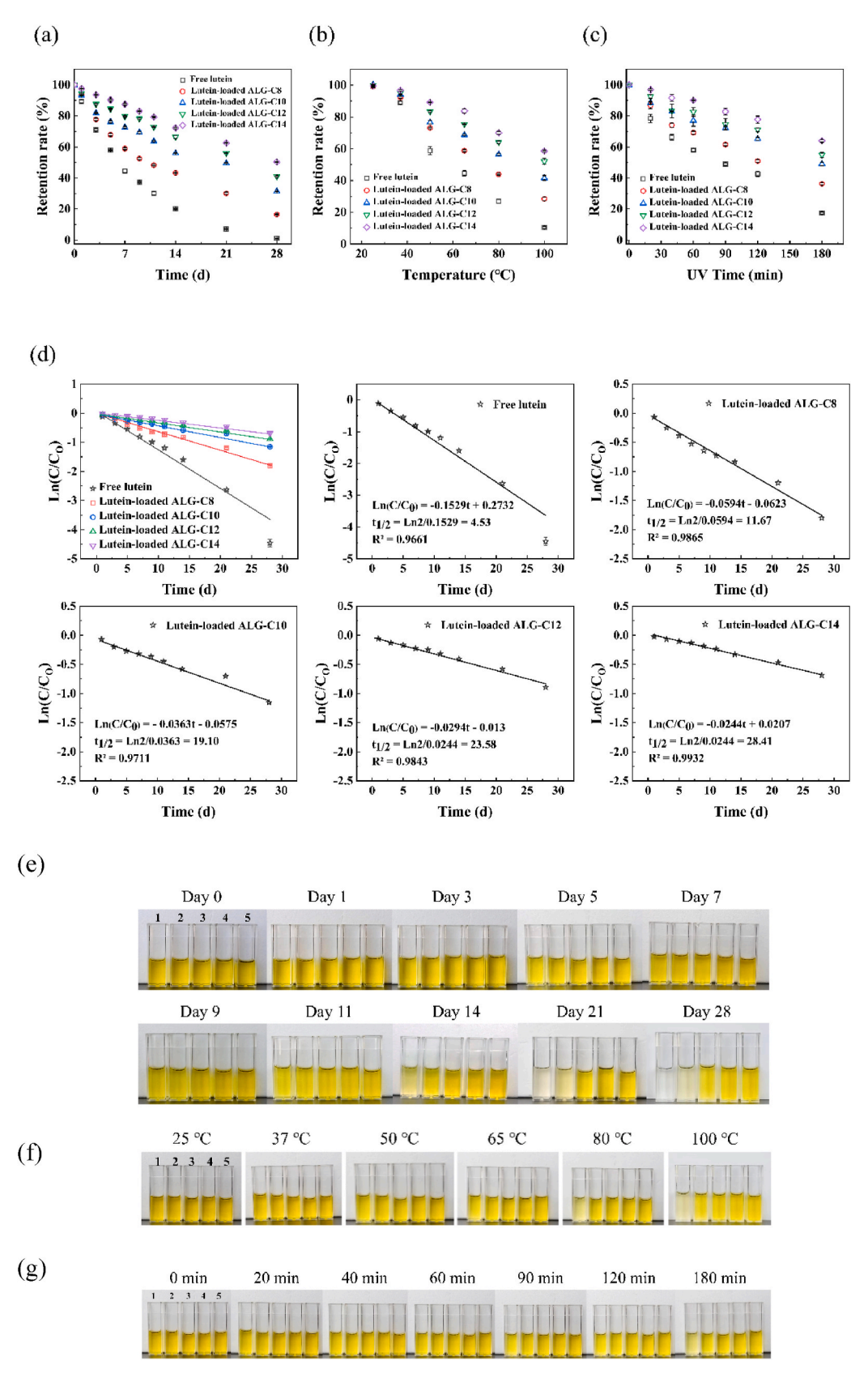
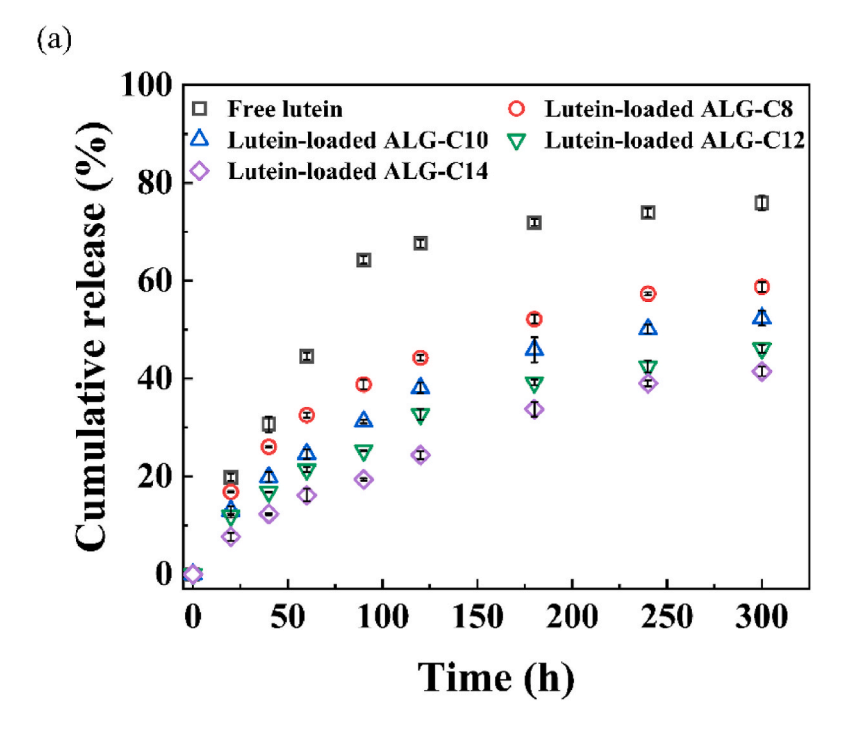


Fig. 4. Schematic diagrams of nanofibers following exposure to environmental stress. Effects of (a) storage time, (b) temperature, and (c) UV irradiation on stability; (d) Light degradation kinetics; (e) lutein retention at different time points (1, 2, 3, 4, and 5 represent free lutein and lutein-loaded ALG-C8, ALG-C10, ALG-C12, and ALG-C14, respectively); (f) lutein retention at different temperatures (1, 2, 3, 4, and 5 represent free lutein and lutein-loaded ALG-C8, ALG-C10, ALG-C12, and ALG-C14, respectively); and (g) lutein retention under UV radiation (1, 2, 3, 4, and 5 represent free lutein and lutein-loaded ALG-C8, ALG-C10, ALG-C12, and ALG-C14, respectively). Data are shown as mean \pm SD (n = 3).

lutein retention in the aggregates were 16.5%, 31.5%, 41.0%, and 50.3%, respectively, at day 28, indicating the protection afforded by the micellar-like aggregates. The degradation of lutein, both free and within the aggregates, followed pseudo-first-order kinetic behavior, with the kinetic rate coefficients shown in Fig. 4d. The k-value denotes the proportional degradation rate of a substance, whereas extended half-lives ($t_1/2$) signify a more gradual degradation process (Liu, Ma, et al., 2024). Free lutein and lutein loaded into ALG-C8, ALG-C10, ALG-C12, and ALG-C14 micellar-like aggregates were found to have half-lives of 4.5, 11.7, 19.1, 23.6, and 28.4 days, respectively. This indicates that

encapsulation of lutein within the micellar-like aggregates markedly enhanced its photostability, especially in the case of the ALG-C14 aggregates. In commercial applications, particularly in the manufacture of liquid materials, thermal sterilization is frequently used as a protection against bacterial contamination (Liu, Ma, et al., 2024). However, lutein is known to be degraded by high temperatures during food processing. Fig. 4b displays the retention of free and encapsulated lutein after 30 min of treatment at different temperatures. The color changes observed in the samples are illustrated in Fig. 4f. The proportions of free lutein retained were 44.6 % and 10.4 % following pasteurization (65 °C) and



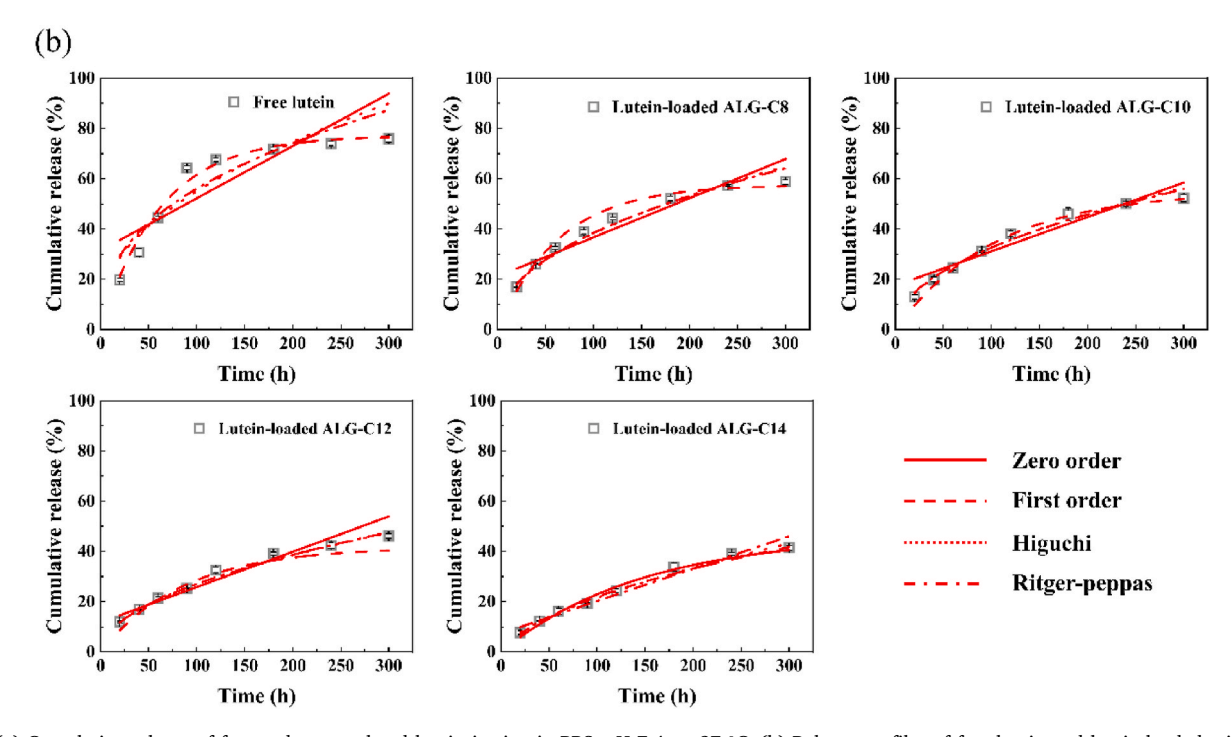


Fig. 5. (a) Cumulative release of free and encapsulated lutein *in vitro* in PBS, pH 7.4, at 37 °C; (b) Release profiles of free lutein and lutein-loaded micellar-like aggregates. Data are shown as mean \pm SD (n = 3).

boiling sterilization (100 °C), respectively. Notably, at 100 °C, the retention of lutein in micellar-like aggregates was 28.5 %, 41.6 %, 52.0 %, and 58.6 %, respectively. Fig. 4c illustrates the influence of UV-light on lutein. The sample colors and their absorbances are shown in Fig. 4g. It was observed that free lutein degraded rapidly following exposure to UV light for 3 h, yielding a retention rate of 17.5 %. However, the presence of the aggregates protected the lutein from decomposition due to UV light. After 3 h of UV-light irradiation, the lutein retention in the aggregates was 36.3 %, 49.1 %, 54.9 %, and 63.9 %, respectively, with the lutein in the ALG-C14 aggregate showing the greatest retention. It is thus apparent that the protective layer provided by the derivatives mitigated lutein degradation caused by light, temperature, and UV exposure, resulting in stability under conditions of environmental stress and enhancing its bioavailability during *in vivo* release.

3.5. Lutein release from micellar-like aggregates

The in vitro release of lutein from the aggregates in PBS (pH 7.4) at 37 °C was investigated, with the cumulative release profiles illustrated in Fig. 5a. Free lutein showed a burst release (about 64.3 %) within 1.5 h, with the release rate increasing to 75.9 % at 5 h. During the initial 2.0 h, there was a rapid release of lutein from the aggregates, with release rates of 24.4 %, 32.7 %, 38.1 %, and 44.3 %, respectively. The explanation for this may be that some lutein adsorbed on the aggregate surface is released through free diffusion (Yan, et al., 2019, 2020). Furthermore, the initial rapid release of lutein may also have been attributed to the multiple microdomain structures of the aggregates (Liu, Ma, et al., 2024). The release rate then slowed downtrend, likely the result of lutein release from the hydrophobic cores of the aggregates, with reduced release rates corresponding to the lutein concentrations within the core (Liu et al., 2022). Images of lutein release at different time points are given in Fig. S3. The coloration of the solutions is indicative of the quantity of lutein released.

The data were subjected to analysis via multiple fitting models, such as zero-order, first-order, Higuchi, and Ritger-Peppas models (Fig. 5b and Table 2). The First-order, Higuchi, and Ritger-Peppas equations all showed satisfactory fitting performance. In particular, the Ritger-Peppas equation demonstrated the best fit, with R2 values closest to 1. Specifically, the R2 values for lutein-loaded ALG-C8, ALG-C10, ALG-C12, and ALG-C14 aggregates were 0.989, 0.984, 0.991, and 0.991, respectively. Furthermore, the mechanism by which lutein is released could be analyzed with the Ritger-Peppas model if the cumulative rate did not exceed 60 % (Liu, Ma, et al., 2024). According to the model, n < 0.45corresponds to Fickian diffusion behavior, 0.45 < n < 0.89 denotes anomalous (non-Fickian) diffusion mechanisms, a value of n = 0.89 represents Case-II transport mechanism (zero-order release), and n > 0.89 represents Super-Case-II transport (Yang et al., 2021). The characteristic index (n) values for lutein release from ALG-C8, ALG-C10, ALG-C12, and ALG-C14 aggregates were 0.468, 0.490, 0.517, and 0.634, respectively, suggesting that lutein release conformed to the non-Fickian diffusion model. This finding implies that the diffusion of loaded lutein is influenced by micellar-like aggregates with varying alkyl chain lengths, collectively controlling the rate of lutein release. These results indicated that micellar-like aggregates with the longest alkyl chains had the strongest hydrophobic interactions with lutein and thus a more controlled release effect (Shen et al., 2021). Therefore, the lutein-loaded aggregates were able to release lutein continuously, leading to prolongation of its survival in physiological environments and thus enhancing its bioavailability.

3.6. Assessment of cytotoxicity of derivatives in vitro

An *in vitro* assessment of the potential cytotoxic potential of sodium alginate and its derivatives was performed using MTT assays on RAW 264.7 cells. Typically, cell viability over 80 % as assessed in MTT assays is indicative of low cytotoxicity (Liu et al., 2022). As shown in Table 3,

Table 2The fitted equations for the kinetics of lutein release.

Sample	Model	Equation	R^2	Release mechanism
Free lutein	Zero order	$Qt = 0.208t + \\ 31.404$	0.663	Fickian diffusion
	First order	Qt = 77.150(1-exp(-0.016t))	0.975	
	Higuchi	$Qt = 4.772t^{1/2} + 7.269$	0.825	
	Ritger- Peppas	$Qt = 8.743t^{0.403}$	0.848	
Lutein-loaded ALG- C8 micellar-like	Zero order	$Qt = 0.156t + \\ 21.065$	0.979	Non-Fickian diffusion
aggregate	First order	Qt = 57.597(1-exp(-0.015t))	0.985	
	Higuchi	$Qt = 3.644t^{1/2} + 1.708$	0.987	
	Ritger- Peppas	$Qt = 4.458t^{0.468}$	0.989	
Lutein-loaded ALG- C10 micellar-like	Zero order	Qt = 0.137t + 17.459	0.898	Non-Fickian diffusion
aggregate	First order	Qt = 55.056(1-exp(-0.010t))	0.979	
	Higuchi	$Qt = 3.260t^{1/2}$ $^{2}-0.046$	0.984	
	Ritger- Peppas	$Qt = 3.413t^{0.490}$	0.984	
Lutein-loaded ALG- C12 micellar-like	Zero order	$\begin{array}{l} Qt = 0.140t \ + \\ 11.761 \end{array}$	0.941	Non-Fickian diffusion
aggregate	First order	Qt = 41.641(1-exp(-0.012t))	0.902	
	Higuchi	$Qt = 2.776t^{1/}$ 2 -0.731	0.990	
	Ritger- Peppas	$Qt = 2.501t^{0.517}$	0.991	
Lutein-loaded ALG- C14 micellar-like	Zero order		Non-Fickian diffusion	
aggregate	First order	Qt = 46.654(1-exp(-0.007t))	0.952	
	Higuchi	$Qt = 2.704t^{1/}$ 2 -5.107	0.984	
	Ritger- Peppas	$Qt = 1.161t^{0.634}$	0.991	

the survival rate of RAW 264.7 cells exceeded 95 % after 24 h of incubation with sodium alginate and its derivatives at concentrations ranging from 0 to $1000~\mu g/mL$. Cell viability following incubation with the derivatives was comparable to that of sodium alginate, indicating that the incorporation of alkyl chains did not augment cytotoxicity. These findings illustrate the biocompatibility of sodium alginate derivatives and their potential for application in other delivery systems. (Liu et al., 2021).

4. Conclusion

In this study, ¹H NMR and FTIR characterization confirmed the successful synthesis of amphiphilic sodium alginate-based derivatives with varying alkyl chain lengths. The CAC values and sizes of these derivatives decreased as the side-chain lengths at similar DS increased. The morphology of the micellar-like aggregates as shown by TEM was homogeneous with bead-like structures. Furthermore, successful encapsulation of the hydrophobic food component, lutein, in the aggregates was performed using an ultrasonic-dialysis technique. The micellar-like aggregates formed by the derivative with the longest alkyl chain, ALG-C14, showed the highest EE and LC values, specifically, 89.0 \pm 1.58 % and 11.78 \pm 0.18 %, respectively. The micellar-like aggregates were found to protect the encapsulated lutein from adverse environmental conditions, including light, high temperature, and exposure to UV radiation, and released lutein continuously in PBS at pH 7.4 at 37 °C, thus enhancing the bioavailability of lutein and extending its circulation in physiological environments. The release of lutein from the aggregates

Table 3 Viability of RAW 264.7 cells following 24-h culture with sodium alginate and its derivatives at varying concentrations. Data are presented as mean \pm SD (n = 3).

Sodium Alginate 100.66 ± 4.02^a 102.55 ± 3.98^a 99.98 ± 1.79^a 100.24 ± 1.37^a 100.34 ± 2.43^a 101.90 ± 2.44^a ALG-C8 101.11 ± 5.40^a 100.37 ± 1.93^a 100.73 ± 1.89^a 99.37 ± 2.06^a 99.22 ± 1.61^a 100.53 ± 2.37^a ALG-C10 101.03 ± 1.08^a 100.18 ± 0.99^a 101.75 ± 1.13^a 99.57 ± 1.06^a 99.07 ± 2.50^a 100.37 ± 2.19^a ALG-C12 100.98 ± 3.19^a 100.19 ± 3.90^a 100.88 ± 1.87^a 98.75 ± 3.03^a 97.98 ± 0.86^a 99.71 ± 2.47^a	Sample/ Concentration	Cell Viability of 0 μg/ mL Sample (%)	Cell Viability of 200 μg/mL Sample (%)	Cell Viability of 400 µg/mL Sample (%)	Cell Viability of 600 μg/mL Sample (%)	Cell Viability of 800 μg/mL Sample (%)	Cell Viability of 1000 μg/mL Sample (%)
	ALG-C8 ALG-C10	$101.11 \pm 5.40^{a} \\ 101.03 \pm 1.08^{a}$	$100.37 \pm 1.93^{a} 100.18 \pm 0.99^{a}$	$\begin{array}{c} 100.73 \pm 1.89^a \\ 101.75 \pm 1.13^a \end{array}$	$\begin{array}{l} 99.37 \pm 2.06^{a} \\ 99.57 \pm 1.06^{a} \end{array}$	$\begin{array}{l} 99.22 \pm 1.61^{a} \\ 99.07 \pm 2.50^{a} \end{array}$	$100.53 \pm 2.37^{a} 100.37 \pm 2.19^{a}$

Annotation: Data are presented as mean \pm SD (n = 3), Different lowercase letters represent significant differences (p < 0.05).

in vitro followed the non-Fickian diffusion model. The lutein-loaded aggregates could release lutein continuously, prolonging its survival in physiological environments and thus enhancing its bioavailability. Furthermore, the derivatives were not cytotoxic to RAW 264.7 cells, demonstrating their biocompatibility. The findings of this study indicate the potential of these micellar-like aggregates in the food industry for enhancing the stability and bioavailability of lutein, providing a novel, straightforward, and cost-effective approach for the encapsulation of food ingredients.

CRediT authorship contribution statement

Lingyu Han: Writing – review & editing, Writing – original draft, Methodology, Investigation, Formal analysis. Ruiyi Zhai: Writing – review & editing, Writing – original draft, Methodology, Investigation. Peter A. Williams: Writing – review & editing, Methodology, Formal analysis, Conceptualization. Nuo Dong: Writing – review & editing, Software, Methodology, Conceptualization. Jixin Yang: Writing – review & editing, Methodology, Conceptualization. Bing Hu: Writing – review & editing, Writing – original draft, Methodology, Conceptualization.

Declaration of competing interest

Professor Peter A. Williams is the Editor-in-Chief of Food Hydrocolloids and consequently the manuscript should be assigned to Professor Fang Zhong.

Acknowledgements

This article was funded by National Natural Science Foundation of China (No. 32202232), Fundamental Research Funds for the Central Universities (044420250051), and Key research and Development Project of Liaoning Province (2024JH2/102400055).

Appendix A. Supplementary data

Supplementary data to this article can be found online at https://doi.org/10.1016/j.foodhyd.2025.112109.

Data availability

No data was used for the research described in the article.

References

- Atanase, L. I. (2021). Micellar drug delivery systems based on natural biopolymers. Polymers, 13(3).
- Bhat, I., Yathisha, U. G., Karunasagar, I., & Mamatha, B. S. (2020). Nutraceutical approach to enhance lutein bioavailability via nanodelivery systems. *Nutrition Reviews*, 78(9), 709–724.
- Fan, Y. T., Gan, C., Zhang, H. L., & Yi, J. (2024). Characteristics, physicochemical stability and in vitro release of curcumin-loaded glycated bovine serum albumin nanofibrils: Effects of molecular weight of saccharide. Food Hydrocolloids, 155.
- Gupta, R., Chen, Y., & Xie, H. (2021). In vitro dissolution considerations associated with nano drug delivery systems. WIREs Nanomedicine and Nanobiotechnology, 13(6).

- Han, L. Y., Ratcliffe, I., & Williams, P. A. (2017). Synthesis, characterisation and physicochemical properties of hydrophobically modified inulin using long-chain fatty acyl chlorides. *Carbohydrate Polymers*, 178, 141–146.
- Han, L. Y., Sun, J., Williams, P. A., Yang, J. X., & Zhang, S. B. (2022). Octenyl-succinylated inulins for the delivery of hydrophobic drug. *International Journal of Biological Macromolecules*, 221, 1112–1120.
- Han, L. Y., Zhai, R. Y., Hu, B., Williams, P. A., Yang, J. X., Zhang, C. Z., Dong, N., & Li, T. T. (2024). Preparation and characterization of hydrophobically-modified sodium alginate derivatives as carriers for fucoxanthin. Food Hydrocolloids, 157, Article 110386.
- Han, L., Zhai, R., Williams, P. A., Hu, B., Yang, J., Dong, N., Ban, Y., & Li, T. (2025). Hydrophobic derivatization of sodium alginate for use in fucoxanthin delivery. *Food Hydrocolloids*, 170, Article 111664.
- Hao, J., Xu, J. Z., Zhang, W. G., Li, X. Y., Liang, D. D., Xu, D. X., Cao, Y. P., & Sun, B. G. (2022). The improvement of the physicochemical properties and bioaccessibility of lutein microparticles by electrostatic complexation. *Food Hydrocolloids*, 125, Article 107381.
- Li, B., Han, L., Ma, J., Zhao, M., Yang, B., Xu, M., Gao, Y., Xu, Q., & Du, Y. (2023). Synthesis of acylated derivatives of chitosan oligosaccharide and evaluation of their potential antifungal agents on Fusarium oxysporum. *Carbohydrate Polymers*, 314, Article 120955
- Li, H. C., Song, J. L., Liu, C. Y., Wang, X. N., Liu, Y. Y., Han, M. Z., Liang, J., & Gao, Z. P. (2024). Corn starch/β-Cyclodextrin composite nanoparticles for encapsulation of tea polyphenol and development of oral targeted delivery systems with pH-responsive properties. Food Hydrocolloids, 151, Article 109823.
- Li, H., Yuan, Y. K., Zhu, J. X., Wang, T., Wang, D. F., & Xu, Y. (2020). Zein/soluble soybean polysaccharide composite nanoparticles for encapsulation and oral delivery of lutein. Food Hydrocolloids, 103, Article 105715.
- Liu, Z. W., Chen, X. Q., Huang, Z. Q., Shi, J. J., Liu, C. Y., Cao, S. R., Yan, H. Q., & Lin, Q. (2021). Self-assembled oleylamine grafted alginate aggregates for hydrophobic drugs loading and controlled release. *International Journal of Polymeric Materials and Polymeric Biomaterials*, 72(3), 212–223.
- Liu, Z. W., Chen, X. Q., Huang, Z. Q., Wang, H. C., Cao, S. R., Liu, C. Y., Yan, H. Q., & Lin, Q. (2022). One-pot synthesis of amphiphilic biopolymers from oxidized alginate and self-assembly as a carrier for sustained release of hydrophobic drugs. *Polymers*, 14(4), 694.
- Liu, Y. J., Ma, L. Y., Guo, Y. J., Kuang, H. Y., & Liu, Y. X. (2024). Fabricating oleic acid-ovalbumin complexes using an ultrasonic-coupled weakly alkaline pH technique: Improving the dispersibility, stability, and bioaccessibility of lutein in water. Food Chemistry, 435, Article 137593.
- Liu, J. R., Tan, J., Hua, X., Jiang, Z. M., Wang, M. M., Yang, R. J., & Cao, Y. P. (2020). Interfacial properties of ultrahigh methoxylated pectin. *International Journal of Biological Macromolecules*, 152, 403–410.
- Liu, Z. W., Wang, H. C., Bu, Y. N., Wu, T., Chen, X. Q., Yan, H. Q., & Lin, Q. (2024). Fabrication of self-assembled micelles based on amphiphilic oxidized sodium alginate grafted oleoamine derivatives via schiff base reduction amination reaction for delivery of hydrophobic food active ingredients. *International Journal of Biological Macromolecules*, 257.
- Shen, F., Ling, H., Ge, W. J., Yang, Y., Wang, X. Y., Ren, J. L., & Wang, X. H. (2021). Self-assembly behavior and conformation of amphiphilic hemicellulose-graft-fatty acid micelles. Carbohydrate Polymers, 261, Article 117886.
- Wu, Z., Li, H., Zhao, X. W., Ye, F. Y., & Zhao, G. H. (2022). Hydrophobically modified polysaccharides and their self-assembled systems: A review on structures and food applications. *Carbohydrate Polymers*, 284.
- Xu, Y. Y., Li, X. T., Dai, Z. Q., Zhang, Z. Y., Feng, L., Nie, M. M., Liu, C. Q., Li, D. J., & Zhang, M. (2023). Study on the relationship between lutein bioaccessibility and in vitro lipid digestion of nanostructured lipid carriers with different interface structures. Food Hydrocolloids, 139, Article 108569.
- Yan, H. Q., Chen, X. Q., Bao, C. L., Yi, J. L., Lei, M. Y., Ke, C. R., Zhang, W., & Lin, Q. (2020). Synthesis and assessment of CTAB and NPE modified organomontmorillonite for the fabrication of organo-montmorillonite/alginate based hydrophobic pharmaceutical controlled-release formulation. *Colloids and Surfaces, B: Biointerfaces*, 191, Article 110983.
- Yan, H. Q., Chen, X. Q., Feng, M. X., Shi, Z. F., Zhang, W., Wang, Y., Ke, C. R., & Lin, Q. (2019). Entrapment of bacterial cellulose nanocrystals stabilized pickering emulsions droplets in alginate beads for hydrophobic drug delivery. *Colloids and Surfaces B: Biointerfaces*, 177, 112–120.

- Yang, J., Zhou, Q. W., Huang, Z. H., Gu, Z. B., Cheng, L., Qiu, L., & Hong, Y. (2021). Mechanisms of *in vitro* controlled release of astaxanthin from starch-based double
- emulsion carriers. *Food Hydrocolloids, 119,* Article 106837.

 Zhang, F. Q., Xu, H. M., Chen, Z. J., Li, T. T., Li, X. J., Zhou, D. D., Wu, C., & Fan, G. J. (2024). Exploring the binding process of lutein with hydroxypropyl-β-cyclodextrin:
- Multispectral and molecular simulation study. Food Hydrocolloids, 156, Article
- Multispectat and Medical Polymers
 110293.
 Zhang, C. C., Zhang, Y., Song, J. F., Wang, H. J., Wu, C., & Li, Y. (2024). Delivery of lutein by using modified burdock polysaccharide aggregates: Preparation, characterization, and *In Vitro* release properties. *Polymers*, 16(14).